

Spectral behavior of partially pumped weakly scattering random lasers

Jonathan Andreasen^{1,2*} and Hui Cao^{1,3}

¹Department of Applied Physics, Yale University, New Haven, Connecticut 06520, USA

²Laboratoire de Physique de la Matière Condensée, CNRS UMR 6622,
Université de Nice-Sophia Antipolis, Parc Valrose, 06108, Nice Cedex 02, France

³Department of Physics, Yale University, New Haven, Connecticut 06520, USA

jonathan.andreasen@unice.fr

Abstract: Stochastic noise is incorporated in the numerical simulation of weakly scattering random lasers, which qualitatively captures lasing phenomena that have been observed experimentally. We examine the behavior of the emission spectrum while pumping only part of the entire one-dimensional random system. A decrease in the density of lasing states is the dominant mechanism for observing discrete lasing peaks when absorption exists in the unpumped region. Without such absorption, the density of lasing states does not reduce as dramatically but the statistical distribution of (linear) lasing thresholds is broadened. This may facilitate incremental observation of lasing in smaller-threshold modes in the emission spectrum with fine adjustments of the pumping rate.

© 2011 Optical Society of America

OCIS codes: (140.3460) Lasers; (030.4070) Modes; (260.2710) Inhomogeneous optical media.

References and links

1. V. S. Letokhov, "Generation of light by a scattering medium with negative resonance absorption," *Sov. Phys. JETP* **26**, 835–840 (1968).
2. V. M. Markushev, V. F. Zolin, and C. M. Briskina, "Powder laser," *Zh. Prikl. Spektrosk.* **45**, 847–849 (1986).
3. C. Guedard, D. Husson, and C. Sauteret, "Generation of spatially incoherent short pulses in laser-pumped neodymium stoichiometric crystals and powders," *J. Opt. Soc. Am. B* **10**, 2358–2363 (1993).
4. N. M. Lawandy, R. M. Balachandran, A. S. L. Gomes, and E. Sauvain, "Laser action in strongly scattering media," *Nature* **368**, 436–438 (1994).
5. W. L. Sha, C.-H. Liu, and R. R. Alfano, "Spectral and temporal measurements of laser action of rhodamine 640 dye in strongly scattering media," *Opt. Lett.* **19**, 1922–1924 (1994).
6. M. A. Noginov, H. J. Caulfield, N. E. Noginova, and P. Venkateswarlu, "Line narrowing in the dye solution with scattering centers," *Opt. Commun.* **118**, 430–437 (1995).
7. D. S. Wiersma, M. P. van Albada, and A. Lagendijk, "Random laser?" *Nature* **373**, 203–204 (1995).
8. H. Cao, Y. G. Zhao, H. C. Ong, S. T. Ho, J. Y. Dai, J. Y. Wu, and R. P. H. Chang, "Ultraviolet lasing in resonators formed by scattering in semiconductor polycrystalline films," *Appl. Phys. Lett.* **73**, 3656–3658 (1998).
9. H. Cao, Y. G. Zhao, S. T. Ho, E. W. Seelig, Q. H. Wang, and R. P. H. Chang, "Random laser action in semiconductor powder," *Phys. Rev. Lett.* **82**, 2278–2281 (1999).
10. S. V. Frolov, Z. V. Vardeny, K. Yoshino, A. Zakhidov, and R. H. Baughman, "Stimulated emission in high-gain organic media," *Phys. Rev. B* **59**, R5284–R5287 (1999).
11. Y. Ling, H. Cao, A. L. Burin, M. A. Ratner, X. Liu, and R. P. H. Chang, "Investigation of random lasers with resonant feedback," *Phys. Rev. A* **64**, 063808 (2001).
12. X. Wu, W. Fang, A. Yamilov, A. A. Chabanov, A. A. Asatryan, L. C. Botten, and H. Cao, "Random lasing in weakly scattering systems," *Phys. Rev. A* **74**, 053812 (2006).
13. C. Vanneste and P. Sebbah, "Selective excitation of localized modes in active random media," *Phys. Rev. Lett.* **87**, 183903 (2001).

14. X. Jiang and C. M. Soukoulis, "Localized random lasing modes and a path for observing localization," *Phys. Rev. E* **65**, 025601 (2002).
15. C. Vanneste, P. Sebbah, and H. Cao, "Lasing with resonant feedback in weakly scattering random systems," *Phys. Rev. Lett.* **98**, 143902 (2007).
16. M. Patra, "Decay rate distributions of disordered slabs and application to random lasers," *Phys. Rev. E* **67**, 016603 (2003).
17. V. M. Apalkov and M. E. Raikh, "Universal fluctuations of the random lasing threshold in a sample of a finite area," *Phys. Rev. B* **71**, 054203 (2005).
18. A. Yamilov, X. Wu, H. Cao, and A. L. Burin, "Absorption-induced confinement of lasing modes in diffusive random media," *Opt. Lett.* **30**, 2430–2432 (2005).
19. X. Wu, J. Andreasen, H. Cao, and A. Yamilov, "Effect of local pumping on random laser modes in one dimension," *J. Opt. Soc. Am. B* **24**, A26–A33 (2007).
20. J. Andreasen, C. Vanneste, L. Ge, and H. Cao, "Effects of spatially nonuniform gain on lasing modes in weakly scattering random systems," *Phys. Rev. A* **81**, 043818 (2010).
21. P. Sebbah and C. Vanneste, "Random laser in the localized regime," *Phys. Rev. B* **66**, 144202 (2002).
22. M. Terraneo and I. Guarneri, "Distribution of resonance widths in localized tight-binding models," *Eur. Phys. J. B* **18**, 303–309 (2000).
23. F. A. Pinheiro, M. Rusek, A. Orłowski, and B. A. van Tiggelen, "Probing anderson localization of light via decay rate statistics," *Phys. Rev. E* **69**, 026605 (2004).
24. A. D. Mirlin, "Statistics of energy levels and eigenfunctions in disordered systems," *Phys. Rep.* **326**, 259–382 (2000).
25. A. A. Chabanov, Z. Q. Zhang, and A. Z. Genack, "Breakdown of diffusion in dynamics of extended waves in mesoscopic media," *Phys. Rev. Lett.* **90**, 203903 (2003).
26. L. I. Deych, "Effects of spatial nonuniformity on laser dynamics," *Phys. Rev. Lett.* **95**, 043902 (2005).
27. J. Andreasen, A. Asatryan, L. Botten, M. Byrne, H. Cao, L. Ge, L. Labonté, P. Sebbah, A. D. Stone, H. E. Türeci, and C. Vanneste, "Modes of random lasers," *Adv. Opt. Photon.* **3**, 88–127 (2011).
28. G. van Soest, M. Tomita, and A. Lagendijk, "Amplifying volume in scattering media," *Opt. Lett.* **24**, 306–308 (1999).
29. M. Bahoura, K. J. Morris, G. Zhu, and M. A. Noginov, "Dependence of the neodymium random laser threshold on the diameter of the pumped spot," *IEEE J. Quantum Electron.* **41**, 677–685 (2005).
30. E. V. Chelnokov, N. Biturkin, I. Ozerov, and W. Marine, "Two-photon pumped random laser in nanocrystalline ZnO," *Appl. Phys. Lett.* **89**, 171119 (2006).
31. H. Cao, X. Jiang, Y. Ling, J. Y. Xu, and C. M. Soukoulis, "Mode repulsion and mode coupling in random lasers," *Phys. Rev. B* **67**, 161101 (2003).
32. H. E. Türeci, L. Ge, S. Rotter, and A. D. Stone, "Strong interactions in multimode random lasers," *Science* **320**, 643–646 (2008).
33. X. Jiang and C. M. Soukoulis, "Time dependent theory for random lasers," *Phys. Rev. Lett.* **85**, 70–73 (2000).
34. J. Andreasen and H. Cao, "Finite-difference time-domain formulation of stochastic noise in macroscopic atomic systems," *J. Lightwave Technol.* **27**, 4530–4535 (2009).
35. X. Wu and H. Cao, "Statistical studies of random-lasing modes and amplified-spontaneous-emission spikes in weakly scattering systems," *Phys. Rev. A* **77**, 013832 (2008).
36. X. Wu, A. Yamilov, H. Noh, H. Cao, E. W. Seelig, and R. P. H. Chang, "Random lasing in closely packed resonant scatterers," *J. Opt. Soc. Am. B* **21**, 159–167 (2004).
37. A. Taflov and S. Hagness, *Computational Electrodynamics*, 3rd ed. (Artech House, 2005).
38. J. Andreasen, H. Cao, A. Taflov, P. Kumar, and C. qi Cao, "Finite-difference time-domain simulation of thermal noise in open cavities," *Phys. Rev. A* **77**, 023810 (2008).
39. D. M. Sullivan, *Electromagnetic Simulation Using the FDTD Method* (IEEE Press, 2000).
40. R. W. Ziolkowski, J. M. Arnold, and D. M. Gogny, "Ultrafast pulse interactions with two-level atoms," *Phys. Rev. A* **52**, 3082–3094 (1995).
41. P. D. Drummond and M. G. Raymer, "Quantum theory of propagation of nonclassical radiation in a near-resonant medium," *Phys. Rev. A* **44**, 2072–2085 (1991).
42. A. E. Siegman, *Lasers* (University Science Books, 1986).
43. G. J. de Valcárcel, E. Roldán, and F. Prati, "Semiclassical theory of amplification and lasing," *Rev. Mex. Fis.* **52**, 198–214 (2006).
44. J. Andreasen and H. Cao, "Numerical study of amplified spontaneous emission and lasing in random media," *Phys. Rev. A* **82**, 063835 (2010).
45. P. J. Bardroff and S. Stenholm, "Quantum theory of excess noise," *Phys. Rev. A* **60**, 2529–2533 (1999).
46. J. Andreasen and H. Cao, "Creation of new lasing modes with spatially nonuniform gain," *Opt. Lett.* **34**, 3586–3588 (2009).
47. D. W. Scott, "On optimal and data-based histograms," *Biometrika* **66**, 605–610 (1979).
48. O. Frazão, C. Correia, J. L. Santos, and J. M. Baptista, "Raman fibre Bragg-grating laser sensor with cooperative Rayleigh scattering for strain-temperature measurement," *Meas. Sci. Technol.* **20**, 045203 (2009).

1. Introduction

After early research on light diffusion with gain [1] the first experiments [2–6] on “random lasers” [7] exhibited strong amplification around the center frequency of the gain spectrum. In subsequent experiments on strongly scattering semiconductor powders and polycrystalline films with gain, emission spectra showed multiple narrow peaks occurring at frequencies other than the gain center frequency [8, 9]. Similar narrow peaks, appearing on top of a broad and featureless spectrum, were also observed in weakly scattering random systems [10–12]. In these cases, only part of the entire spatial region of the random structures was pumped. Increasing the size of the pumped region added more peaks to the spectra and eventually washed out the fine spectral structure completely. Pumping only part of the entire random system seemed essential to observe the discrete lasing peaks in large samples, especially when scattering was relatively weak. The most commonly cited reason for this behavior is that smaller pump areas excite fewer modes so that individual narrow peaks become distinguishable in the spectrum. However, two types of situations occur when partial pumping is employed: (i) significant absorption exists in the unpumped region, (ii) little or no absorption exists in the unpumped region. The change in the spectral density of possible lasing states (DLS) in each case may be different.

For uniform pumping, information concerning resonances of the passive (without gain) system has been widely used to predict lasing behavior. This relies on there being a correspondence between resonances and lasing modes. If scattering is not too weak and pumping is not too high above the lasing threshold, the small-threshold modes show such correspondence [13–15]. As a result, statistical distributions of resonance decay rates have been used to infer the distribution of lasing thresholds [16, 17].

Concerning partial pumping situation (i), lasing mode properties were found to be dictated by the effective system size given by the pumped region plus the absorption length [18]. In this case, spectral behavior of random lasers with respect to pump size is similar to spectral behavior of passive random systems (of effective size) with respect to the system size. Since the number of resonances reduces with the system size, the number of lasing modes should reduce with the size of the pumped region. The frequency spacing of lasing modes should also increase.

Concerning partial pumping situation (ii), the DLS may not reduce significantly with the pump area [19]. It was found [20] that partial pumping in such systems destroys and creates lasing modes. In the strongly scattering regime (where localized modes exist), partial pumping has been shown to allow spatially non-overlapping high-quality resonances to be selected for lasing [13, 21]. In the weakly scattering regime, modes exhibit more spatial and spectral overlap. Such systems also possess a narrower distribution of decay rates due to reduced scattering [22, 23]. The distribution gets even narrower as the system size decreases [24, 25]. Thus, selecting individual modes for lasing in this regime using partial pumping should be more difficult. However, experiments [10–12] consistently show the observation of discrete lasing peaks when the pumped region is small enough. The mechanism responsible for such observations is not well understood.

Several problems exist for predicting random laser behavior using the information of the passive system. Even uniformly distributed optical gain can modify the spatial properties of lasing modes [26]. In weakly scattering systems, which require more gain to achieve lasing (larger lasing thresholds), the correspondence between lasing modes and resonances significantly degrades [27]. In addition, partial pumping has been shown to increase random laser thresholds even further [11, 28–30]. Mode mixing increases as the size of the pumped region reduces in weakly scattering systems without absorption [20]. There is therefore no one-to-one correspon-

dence between lasing modes of the partially pumped system and lasing modes of the uniformly pumped system (or resonances of the passive system). Thus, a partially pumped random laser is expected to behave differently from predictions based on the passive random system. A statistical study of lasing thresholds themselves is therefore necessary to illustrate the difference.

This paper intends to address the question: how can discrete lasing peaks be observed easily in weakly scattering random lasers for both partial pumping situations (i and ii)? Weakly scattering systems have resonances of very similar decay rates and thus, many modes may lase simultaneously. Mode linewidth affects how much they overlap spectrally and therefore if they can be distinguished in the emission spectrum. But even modes with similar lasing thresholds cannot all lase simultaneously due to gain depletion [31, 32]. Thus, we begin with simulations of realistic situations by incorporating laser linewidths, gain saturation, and consequential mode competition effects. Semiclassical laser theory, based on Maxwell's equations, can predict the discrete lasing peaks [13, 33] but not their spectral width because spontaneous emission is not taken into account. Our numerical method incorporates intrinsic noise into the simulation of random lasers and is based on the finite-difference time-domain formulation we recently developed [34]. The number of discrete lasing peaks in the emission spectra for both types of partial pumping is compared with that of uniform pumping for the same random structure. The number of lasing peaks is found to change differently in each case of partial pumping.

We continue with simulations which isolate the effects of partial pumping. This is accomplished by studying the same random systems without gain saturation and noise. It becomes more clear that for both partial pumping situations, the DLS decreases and facilitates the observation of discrete lasing peaks. This is because the number of small-threshold lasing modes decreases and their frequency spacing increases. We also study the statistical distribution of lasing thresholds for both partial pumping situations and compare to the distribution for uniform pumping. Wu *et al.* compared the statistical distribution of resonance decay rates and lasing thresholds under local pumping without absorption [35]. The two distributions, normalized by their respective average values, were very similar. We find that such normalized distributions can be different when there is absorption outside the pumped region. Wu *et al.* also observed the absolute degree of lasing threshold fluctuations increases with a decrease of the pump size [36]. Our numerical calculations reveal that in both partial pumping situations (i and ii) the absolute degree of lasing threshold fluctuations (statistical variation of thresholds from mode to mode) increases with a decrease of the pump size. Along with a change in the DLS, the increased threshold variations may be a significant factor in determining lasing properties of partially pumped random systems.

This paper is organized as follows. In Sec. 2 information concerning the numerical methods employed in this paper is given. In Sec. 3, results of calculations using the stochastic Maxwell-Bloch equations are presented for three cases: uniform pumping, partial pumping without absorption outside the pumped region, and partial pumping with absorption in the unpumped region. An analysis of these systems is carried out in Sec. 4 using a linear gain model and the threshold statistics of such random systems is provided in Sec. 5. A discussion of results and our main conclusions are drawn in Sec. 6.

2. Numerical Methods

2.1. Generation of One-Dimensional Random Structures

The one-dimensional random systems considered are composed of $N = 41$ layers. Dielectric material with index of refraction $n_1 = 1.05$ separated by air gaps ($n_2 = 1$) results in a spatially modulated index of refraction $n(x)$. Outside the random media $n_0 = 1$. The system is randomized by specifying different thicknesses for each of the layers as $d_{1,2} = \langle d_{1,2} \rangle (1 + \eta \zeta)$ where $\langle d_1 \rangle$ and $\langle d_2 \rangle$ are the average thicknesses of the layers, $0 < \eta < 1$ represents the degree of ran-

domness, and ζ is a random number uniformly distributed in $(-1,1)$. The average thicknesses are $\langle d_1 \rangle = 100$ nm and $\langle d_2 \rangle = 200$ nm giving a total average length of $\langle L \rangle = 6100$ nm. The grid origin $x = 0$ is at the left boundary of the structure and the length of the random structure L is normalized to $\langle L \rangle$. The degree of randomness is set to $\eta = 0.9$. The localization length $\langle \xi \rangle = 220$ μm was calculated from the dependence of ensemble-averaged transmittance T on the system lengths L as $\xi^{-1} = -d \langle \ln T \rangle / dL$ and averaged over the wavelength range of interest (500 nm to 750 nm). Different realizations of random structures are generated using different random seeds for ζ .

2.2. Stochastic Maxwell-Bloch equations: FDTD parameters

This method is based on the finite-difference time-domain (FDTD) [37] formulation we recently developed to study the effects of noise on light-atom interaction in complex systems without prior knowledge of resonances [34, 38]. The interference effects of electromagnetic waves and the openness of the system are fully accounted for with Maxwell's equations and exact absorbing boundary conditions [39]. The incorporation of the Bloch equations describes the evolution of the density matrix for two-level atoms and their interaction with light [40]. To introduce noise to the Bloch equations, we use the stochastic c -number equations that are derived from the quantum Langevin equations in the many-atom and many-photon limit [41]. We are interested in the lasing behavior of macroscopic systems so we neglect nonclassical noise and consider only classical noise resulting from the decay, dephasing, and pumping of atoms.

The atomic transition frequency is set to $k_a = 10.5$ μm^{-1} , the corresponding wavelength $\lambda_a = 600$ nm. The lifetime of atoms in the excited state T_1 and the dephasing time T_2 are included in the Bloch equations. The width of the gain spectrum is given by $\Delta k_a = (1/T_1 + 2/T_2)/c$ [42]. We set $T_1 = 1.0$ ps. The value of T_2 is chosen such that the gain spectrum spans ten resonances of the passive system. With an average frequency spacing $\Delta k = 0.5$ μm^{-1} , $\Delta k_a = 5.0$ μm^{-1} , and $T_2 = 1.3$ fs. We also include incoherent pumping of atoms from level 1 to level 2. The rate of atoms being pumped is proportional to the population of atoms in level 1 (ρ_{11}), and the proportionality coefficient P is called the pumping rate. The stochastic simulations solve for the population of excited atomic states ρ_{22} and atomic polarization $\rho_1 = \rho_{12} + \rho_{21}$ and $\rho_2 = i(\rho_{12} - \rho_{21})$. With $T_2 \ll T_1$, we neglect pump fluctuations on the polarization because they are orders of magnitude smaller than noise due to dephasing. The stochastic Maxwell-Bloch (SMB) equations are solved through a parallel FDTD implementation.

2.3. Implementation of Three Pumping Cases

Lasing with uniform pumping is simulated with the SMB equations by distributing two-level atoms uniformly over the entire random system to avoid additional light scattering caused by the spatial inhomogeneity of gain. Although it does not correspond to common experimental situations where gain atoms are incorporated only in the higher-index dielectric layers, it is possible to have gain atoms in the gas phase distributed in the air gaps. The two-level model of atoms is a simplified approach that can be applied to actual lasers based on three-level atoms such as Ruby and Erbium lasers, as the population in the third level is negligibly small [43]. Partial pumping is simulated by placing two-level atoms only in the region $0 \leq x \leq \ell_G$ (still in both the higher-index dielectric layers and the air gaps). We choose $\ell_G/L = 1/3$. In the unpumped region ($x > \ell_G$), there are no atoms nor is there absorption of any kind. There is only scattering due to the passive random structure. In both of these cases, the output field is sampled at the grid point $x = L$ at the right boundary of the random system. We Fourier-transform the output field to obtain the emission spectra.

Partial pumping with absorption in the unpumped region ($x > \ell_G$) is achieved by placing two-level atoms there in the ground state. Light emitted from the pumped region is reabsorbed in the

unpumped region. The average decay length of the intensity in this region yields an absorption length $\ell_a \approx 170$ nm. This is much smaller than the length of the unpumped region ($L - \ell_G = 4067$ nm). With strong absorption and no pumping, the noise terms are small in the unpumped region. We neglect them when the excited state population is less than a threshold value α . Incrementally decreasing α and monitoring the change of physical quantities, we found results to converge when $\alpha = 10^{-12}$. When absorption is included at $x > \ell_G$, fields emitted from the pumped region are significantly absorbed so that no signal reaches $x = L$. Thus, in this case, the field at $x = 0$ is used to obtain the emission spectra. Without absorption, results from sampling at $x = L$ are identical in character to those from sampling at $x = 0$.

With noise terms included in the SMB equations, all quantities fluctuate in time for all pumping cases. For a fixed pumping rate, however, their values averaged over small time windows become nearly constant eventually. By comparing the spectra of output light taken over different temporal windows up to $t = 267$ ps, we find a steady state is reached by 16.6 ps for all pumping rates considered here.

2.4. Transfer Matrix Method

To further understand the nature of lasing modes with uniform and partial pumping, we employ the transfer matrix method developed [20] to find the threshold lasing modes (TLMs) with linear gain. Propagation of the electric field through the structure is calculated via the 2×2 matrix M . Linear gain, independent of frequency, is simulated by appending an imaginary part to the dielectric function $\varepsilon(x) = \varepsilon_r(x) + i\varepsilon_i(x)$, where $\varepsilon_r(x) = n^2(x)$. The complex index of refraction

$$\tilde{n}(x) = \sqrt{n^2(x) + n_y^2(x)} + in_y(x), \quad (1)$$

where $n_y(x) < 0$ for gain and in turn modifies the real part [20].

With uniform pumping, $n_y(x)$ is considered to be spatially constant within the random system. This is similar to the SMB simulations in the previous section and yields a gain length $\ell_g = 1/|n_y|k$ ($k = 2\pi/\lambda$ is the vacuum frequency of a TLM) which is the same in the dielectric layers and the air gaps. Partial pumping is implemented with a step function $n_y(x) = n_i H(-x + \ell_G)$, where $x = 0$ is the left edge of the structure and $x = \ell_G$ specifies the right edge of the pumping region.

Absorption in the unpumped region is implemented through $n_y(x) = (2k\ell_a)^{-1}$, where $n_y(x) > 0$ for absorption and ℓ_a is the absorption length. For partial pumping with absorption $\tilde{n}(x) = n(x) + i(1/2k\ell_a)$ in the unpumped region. Such absorption is not included in the pumped region.

Boundary conditions with only emission out of the system require $\text{Re}[M_{22}] = 0$ and $\text{Im}[M_{22}] = 0$ [20]. These conditions result in “zero lines” formed in the plane of (k, n_i) . The crossing of a real and imaginary zero line in the (k, n_i) plane results in $M_{22} = 0$ at that location. The values of k and n_i at these locations correspond to the frequency and threshold gain of a lasing mode, respectively. The benefit of this method is that the lasing thresholds may be estimated quickly and easily relative to one another. Moreover, without gain saturation and noise included the effects of partial pumping are isolated.

3. Stochastic Maxwell-Bloch Simulations of Random Lasers

3.1. Uniform Pumping

Figure 1 shows the steady-state emission spectra $|E(k)|^2$ for uniform pumping with increasing pumping rates. At a pumping rate of $P_r = 1.00$ [Fig. 1(a)], there is no net gain. The number of ground-state atoms is ρ_{11} and the number of excited-state atoms is ρ_{22} . Without stimulated emission and noise, the number of atoms pumped from the ground to excited state is $P_r\rho_{11}/T_1$. Meanwhile, the decay rate of atoms is ρ_{22}/T_1 . Thus, when $P_r = 1.00$, $\rho_{11} = \rho_{22}$ and the atomic

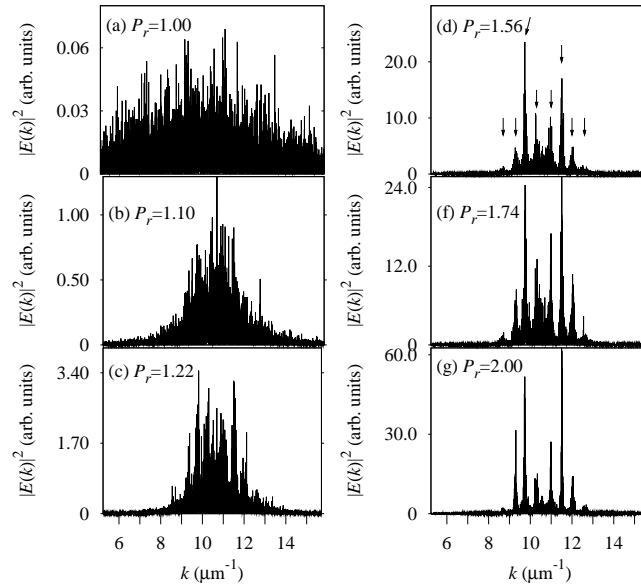


Fig. 1. Steady-state intensity spectra $|E(k)|^2$ for uniform pumping ($\ell_G/L = 1$). (a) $P_r = 1.00$. A broad peak is centered around k_a . (b) $P_r = 1.10$. The broad peak narrows around k_a . (c) $P_r = 1.22$. Multiple peaks appear on top of the broad peak. (d) $P_r = 1.56$. Eight visible peaks are marked with arrows. From (f) $P_r = 1.74$ to (g) $P_r = 2.00$, the dominant peaks are revealed.

system is at the transparency point ($\rho_{22} - \rho_{11} = 0$). Noise reduces the excited state population, and it is just below the transparency point for $P_r = 1.00$. The steady-state emission spectra in this case has a broad peak and is centered at the atomic transition frequency $k_a = 10.5 \mu\text{m}^{-1}$, resembling the spontaneous emission spectrum. On top of it there are many fine spikes whose frequencies change chaotically from one time window of Fourier transform to the next. They result from the stochastic emission process with their spectral width determined by the temporal length of the Fourier transform. We have found [44] such spikes to bear similar statistical characteristics to the experimentally observed ASE spikes.

Above the transparency point at $P_r = 1.10$ [Fig. 1(b)], there is net gain. The broad emission peak grows and narrows spectrally. Since optical gain is frequency dependent, the emission intensity closer to k_a is amplified more than that away from k_a , leading to a spectral narrowing. This behavior is typical of ASE.

As the pumping rate P_r increases [Figs. 1(c) – 1(g)], discrete peaks begin to form amidst the broad emission peak. They correspond to resonances of the passive system. We mark eight visible peaks in Fig. 1(d). The frequency of these peaks is stable with respect to the pumping rate. They also become narrower and more distinct at higher pumping rates. All of these modes are constantly excited by noise and subsequently amplified in the presence of population inversion.

To ensure these results are not limited to the particular configuration considered here, the simulations are repeated with another random seed (to initialize the noise terms) and another realization of a random structure. The results are qualitatively similar. Slight differences arise due to stochasticity.

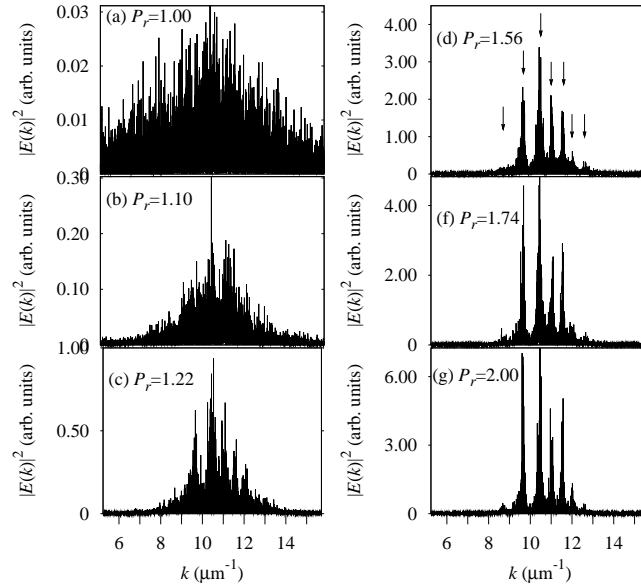


Fig. 2. Steady-state intensity spectra $|E(k)|^2$ for partial pumping ($\ell_G/L = 1/3$). (a) $P_r = 1.00$. A broad peak is centered around k_a . (b) $P_r = 1.10$. The broad peak narrows around k_a and multiple peaks already emerge on top of the broad peak. (c) $P_r = 1.22$. More peaks emerge. (d) $P_r = 1.56$. Seven visible peaks are marked with arrows. From (f) $P_r = 1.74$ to (g) $P_r = 2.00$, the dominant peaks are revealed. The number of modes is less than the case with uniform pumping and the lasing modes are more separated in frequency.

3.2. Partial Pumping

Figure 2 shows the steady-state emission spectra $|E(k)|^2$ for partial pumping with increasing pumping rates. At $P_r = 1.00$ [Fig. 2(a)], the system is near the transparency point ($\rho_{22} - \rho_{11} \lesssim 0$) in the pumped region. The steady-state emission spectra again has a broad featureless peak and is centered at the atomic transition frequency $k_a = 10.5 \mu\text{m}^{-1}$. On top of it there are many fine spikes resulting from the stochastic emission process.

In contrast to the uniform pumping case, resonance peaks are more visible in the emission spectrum for $P_r = 1.10$ [Fig. 2(b)]. These peaks grow as P_r increases further [Figs. 2(c) – 2(g)]. We mark seven visible peaks in Fig. 2(d). The frequency of these peaks is stable with respect to the pumping rate. They also become narrower and well separated due to amplification. There is one less peak here compared to the uniform pumping case, but there appears to be some correspondence between the peak frequencies for partial and uniform pumping. The relation of these peaks to peaks in the uniform pumping case will be examined in detail in Sec. 4.

It is evident that the frequency separation between lasing peaks is increased from the uniform pumping case. Greater frequency separation allows the resonance peaks to be more distinguishable from the broad ASE peak. Spectral overlap has been reduced, but the effect is different from what occurs for stronger scattering. If the index contrast is increased, spectral overlap reduces due to the resonance linewidths becoming narrower. Thus, even if the frequency spacing is the same as weaker scattering, the resonance peaks can be visible in the presence of noise even when there is no net gain [44].

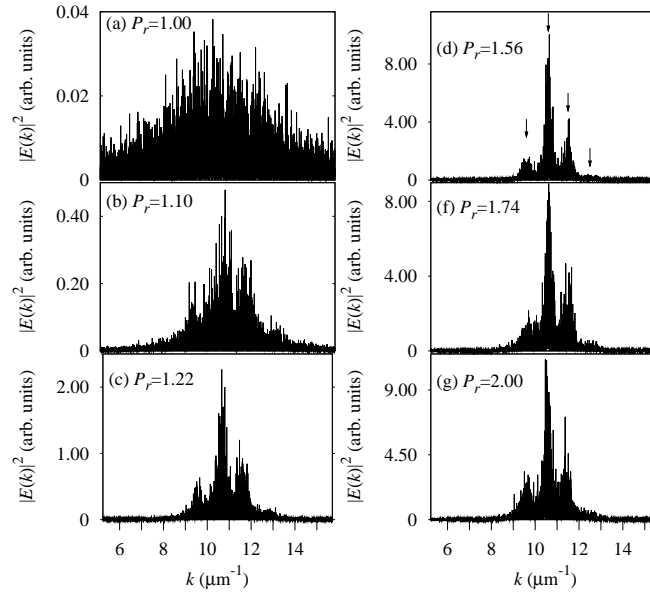


Fig. 3. Steady-state intensity spectra $|E(k)|^2$ for partial pumping ($\ell_G/L = 1/3$) and absorption in the unpumped region ($\ell_a = 170$ nm). (a) $P_r = 1.00$. A broad peak is centered around k_a . (b) $P_r = 1.10$. The broad peak narrows around k_a and multiple peaks already emerge on top of the broad peak. (c) $P_r = 1.22$. More peaks emerge. (d) $P_r = 1.56$. Five visible peaks are marked with arrows. From (f) $P_r = 1.74$ to (g) $P_r = 2.00$, the dominant peaks are revealed. The number of modes is less than the case of partial pumping without absorption and the lasing modes are more separated in frequency.

3.3. Absorption in the Unpumped Region

Figure 3 shows the steady-state emission spectra $|E(k)|^2$ for partial pumping with absorption in the unpumped region as the pumping rate increases. At $P_r = 1.00$ [Fig. 3(a)], near the transparency point in the pumped region, the broad ASE peak is seen at $k_a = 10.5 \mu\text{m}^{-1}$. Like the previous partial pumping case, resonance peaks emerge clearly in the emission spectrum for $P_r = 1.10$ [Fig. 3(b)] and they grow as P_r increases further [Figs. 3(c) – 3(g)]. In contrast to the previous partial pumping case, there are far fewer peaks in the emission spectra with absorption included. We mark four visible peaks in Fig. 3(d). The frequency of these peaks is stable with respect to the variation of the pumping rate. However, the peak frequencies in this case are notably different from those in the uniform and partial pumping cases without absorption. The relation between these peaks will be examined in detail in Sec. 4.

With the number of peaks noticeably reduced, the frequency separation increases further compared to the cause of partial pumping without absorption. The increased frequency separation makes it easier to distinguish the peaks from the broad ASE peak. Although the resonance peaks in Fig. 3 become narrower due to amplification, they are not as narrow as the peaks in the case without absorption. This behavior is consistent with analytical work [45] which shows the amount of excess noise increases when the spatial distributions of gain and loss are different. The excess noise contributes an additional factor to the linewidth.

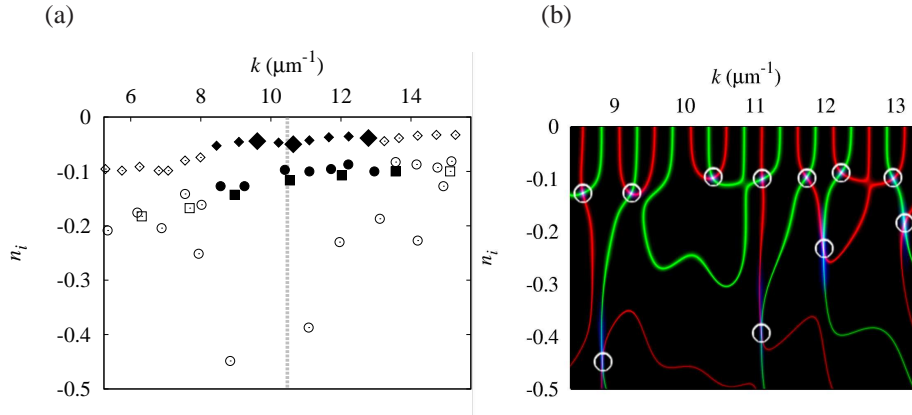


Fig. 4. (Color online) The frequencies k and thresholds n_i of lasing modes with linear gain. (a) TLM solutions for (diamonds) uniform pumping ($\ell_G/L = 1$), (circles) partial pumping ($\ell_G/L = 1/3$), and (squares) partial pumping with absorption in the unpumped region ($\ell_a = 170$ nm). The filled symbols represent the modes which are visible in the emission spectra of the SMB simulations. The enlarged filled diamonds are TLMs for uniform pumping that disappear for partial pumping without absorption. The vertical dashed gray line marks the center frequency of the gain spectrum k_a in the SMB simulations. (b) Real (green) and Imaginary (red) zero lines of M_{22} in the (k, n_i) plane for partial pumping over the frequency range of the filled circles in (a). TLM solutions are marked by white circles.

4. Threshold Lasing Modes With Linear Gain

Figure 4(a) compares lasing frequencies k and thresholds n_i with uniform and partial pumping implemented via Eq. (1). With uniform pumping ($\ell_G/L = 1$), the separation of thresholds between neighboring modes marked by diamonds is quite small. This results in all the modes having very similar behavior as the pumping rate is increased in the SMB simulations in Fig. 1. The eight peaks marked by arrows in Fig. 1(d) are associated with the threshold lasing modes (TLMs) marked by filled diamonds in Fig. 4(a). There are nine filled diamonds because the two TLMs closest to k_a in Fig. 4(a) appear only as a “composite” peak in Fig. 1(d). The finite linewidths of the two modes exceed their frequency spacing, which is reduced by the frequency pulling effect. Consequently, the two modes are indistinguishable and appear to be merged. Nevertheless, there is a clear correspondence between the TLMs and the peaks seen in the SMB simulations. The frequency pulling effect merely shifts the frequencies toward the center of the gain curve in the SMB simulations by 10–20% (compared to the TLM frequencies).

With partial pumping ($\ell_G/L = 1/3$), the lasing thresholds $|n_i|$ increase significantly as illustrated by the circles in Fig. 4(a). The seven peaks marked by arrows in Fig. 2(d) are associated with the TLMs marked by filled circles in Fig. 4(a). Aside from slight frequency pulling ($\sim 16\%$), there is a clear correspondence between the TLMs and the peaks seen in the SMB simulations. The increased frequency separation between the TLMs (e.g., at $k = 9.26 \mu\text{m}^{-1}$ and $k = 10.4 \mu\text{m}^{-1}$) allows them to be visible in the SMB simulations at $P_r = 1.10$ [Fig. 2(b)].

The reason for this increased frequency separation is due to the disappearance of some small threshold modes and the creation of lasing modes with larger thresholds. This process is seen more clearly in Fig. 4(b) which shows the zero lines of the real and imaginary parts of M_{22} . The zero line crossings are marked by circles which correspond to TLM solutions [the same solutions marked by the circles in Fig. 4(a)]. From small to large thresholds (top to bottom), real and imaginary zero lines may cross once but may also cross again at larger thresholds. Thus, two

classes of TLMs can be seen: those associated with first-crossings of the zero lines and those associated with additional crossings. Only the first class of TLMs have any correspondence to TLMs with uniform pumping [20] (though there is mode mixing). The second class of TLMs are actually new lasing modes generated by partial pumping [46]. In general, the first class has smaller lasing thresholds and are usually the modes observed to lase at pumping rates not too high above threshold. For example, the peaks which appear in Fig. 2 are only associated with the first class of modes. This is not always the case since the second class of modes may be observed with specific gain spectrum [46]. Typically, however, the frequencies of the small-threshold lasing modes are observed to become more separated and for small pumping rates there are effectively fewer lasing modes available within a fixed gain spectrum.

Figure 2 shows that there is one less peak with partial pumping compared to uniform pumping. However, Fig. 4(b) reveals that three modes from the uniform pumping case have disappeared. These three modes are marked by enlarged filled diamonds in Fig. 4(a). This means there is not one less but three less modes compared to the uniform pumping case. Only one less peak appears in Fig. 2 because of the composite peak close to k_a (for uniform pumping) and because of an extra higher-frequency mode that shifted from $k = 13.2 \mu\text{m}^{-1}$ to $k = 13 \mu\text{m}^{-1}$. Note that the shift is not caused by frequency pulling because n_i is frequency-independent. This is a shift caused by partial pumping because n_i modifies the real part of the refractive index n_r [some modes shift away from k_a as seen in Fig. 4(a)]. Frequency pulling due to the finite-width gain spectrum in the SMB simulations shifts this mode further to $k = 12.7 \mu\text{m}^{-1}$ in Fig. 2.

To simulate absorption in the unpumped region for the partial pumping case, we use $\ell_a = 170$ nm, which was the approximate absorption length in the SMB simulations in Sec. 3.3. The lasing thresholds n_i shown in Fig. 4(a) increase compared to partial pumping without absorption, as expected. The four peaks marked by arrows in Fig. 3(d) are associated with the TLMs marked by filled squares in Fig. 4(a). More frequency pulling occurs in this case with a shift of 30–40% compared to the TLM frequencies. Nevertheless, there is a clear correspondence between the TLMs and the peaks seen in the SMB simulations.

The reduction in the number of lasing modes results in a large frequency separation and allows them to be distinguishable even in the SMB simulations at $P_r = 1.10$ [Fig. 2(b)]. The reason for the increased frequency separation in this case is entirely different from the partial pumping case without absorption. With absorption, the peaks are associated with modes confined to the pumped region [18]. Thus, in general, they do not correspond to peaks of the uniformly pumped system. In other words, with absorption, the modes are determined only by local region of the random structure of length $\ell_G + \ell_a$. Feedback from the random structure beyond $\ell_G + \ell_a$ is suppressed due to absorption. Without absorption, additional feedback in the unpumped region plays a role in determining the modes.

The other effect that may play a role in lasing with partial pumping is the threshold separation. The class of small-threshold modes for partial pumping in Fig. 4(a), have thresholds which have become more separated due to partial pumping. This greater separation of thresholds would make it easier to see modes begin lasing incrementally with a gradual increase of the pumping rate. Furthermore, if the threshold pumping rate is P_t and the experimentally limited pump step (e.g., by power fluctuations) is ΔP , then the relative pump step is $\delta P = \Delta P / P_t$. Larger P_t means a smaller allowable adjustments of δP , thereby allowing a finer tuning of the pumping rate with respect to the threshold value.

Observations here are based on results from this example of a random structure. In the next section, we study the statistics of lasing thresholds for an ensemble of random structures to obtain more general conclusions.

5. Effects of Inhomogeneous Pumping and Absorption on Threshold Statistics

The effects of partial pumping reveal themselves here through calculations of the lasing threshold statistics of TLMs. We consider 10000 realizations of the random structures described in Sec. 2.1. The right spatial boundary of the gain region ℓ_G [implemented via Eq. (1)] is always chosen to coincide with an interface between the higher-index dielectric material and air. This results in a partial pumping length of $\ell_G/L = 0.33 \pm 0.011$ over the 10000 realizations. With the number of modes reduced by 3 on average in the partial pumping case with absorption, we consider 30000 structure realizations in order to maintain roughly the same number of modes. Different realizations of random structures are generated using different random seeds for ζ . The frequency range for these calculations is limited to $k_a \pm 2 \mu\text{m}^{-1}$, the same range as the SMB simulations in Sec. 3. The solutions are pinpointed precisely by using the Secant method. Locations of minima of $|M_{22}|^2$ and a random value located closely to these minima locations are used as the first two inputs to the Secant method. Once a solution converges or $|M_{22}| < 10^{-12}$, a solution is considered found. Verification of these solutions is provided by the phase of M_{22} , calculated as $\theta = \text{atan2}(\text{Im}M_{22}, \text{Re}M_{22})$. Locations of vanishing M_{22} give rise to phase singularities since both the real and imaginary parts of M_{22} vanish. The phase change around a path surrounding a singularity is $\pm 2\pi$. Thus, if the phase change around a proposed solution is not $\pm 2\pi$, that solution is discarded.

This mode-finding method was tested using 10 different random structures and 10 different random seeds (for the second initial guess used in the Secant method). All solutions were found manually for these cases in order to test the reliability of the Secant method. The crossings of real and imaginary zero lines [e.g., in Fig. 4(b)] are found easily by eye. For uniform pumping, all modes were always found by the Secant method. For partial pumping, 96% of modes were found successfully by the Secant method. Some modes are missed due to sharp modulations of M_{22} . Convergence for these modes is limited numerically by machine precision.

Though the lasing thresholds $n_i < 0$, we hereafter refer $|n_i|$ to n_i for brevity. The optimal bin size Δn_i for lasing thresholds was found using the Scott formula [47] based on the main peak of the distributions. For uniform pumping $\Delta n_i = 0.001$ and for partial pumping $\Delta n_i = 0.002$. The histograms are normalized yielding the probability distribution $P(n_i)$ so that $\int P(n_i)dn_i = 1$.

Figure 5 shows the $P(n_i)$ for uniform and partial pumping. No absorption is included for partial pumping. Figure 5(a) shows a large-threshold tail for $n_i > 0.175$ in the partial pumping case. The reason for the sharp kink between small and large-threshold modes is seen clearly in Fig. 4(b). The large-threshold modes are formed predominantly by secondary crossings of the real and imaginary zero lines of M_{22} . These secondary crossings have n_i well above the first crossings. This tail highly distorts the threshold statistics which is evident in the skewness S that characterizes the degree of asymmetry around the mean value. The skewness increases from $S = 1.4$ for uniform pumping to $S = 2.2$ for partial pumping.

The large-threshold modes rarely lase experimentally, so we only consider data for $n_i \leq 0.175$ with partial pumping and re-normalize the histogram to obtain a new probability distribution. The inset in Fig. 5(a) shows this re-normalized threshold distribution (the distribution for uniform pumping is left unchanged). Due to asymmetry (even uniform pumping has $S > 1$), we characterize the first moment of the distribution using the most probable threshold n_m rather than the mean threshold $\langle n_i \rangle$. n_m shifts from 0.047 for uniform pumping to 0.112 for partial pumping, a factor of 2 increase.

The standard deviation around n_m increases from $\sigma = 0.012$ for uniform pumping to $\sigma = 0.023$ for partial pumping, nearly twice as large. This indicates the fluctuation of thresholds increases for smaller pumping sizes. Furthermore, the inset of Fig. 5(a) shows the slope of the rising part of the re-normalized threshold distribution with partial pumping. The number of lasing modes dN_i within a threshold range dn_i is proportional to the slope m ($dN_i = m dn_i$). With

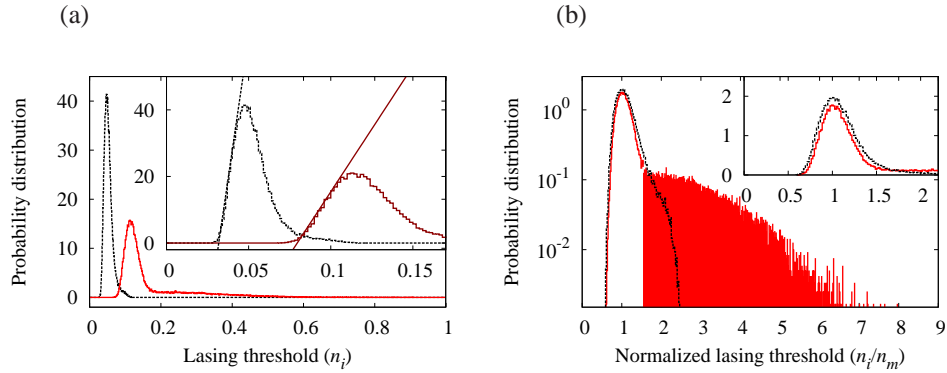


Fig. 5. (Color online) (a) Probability distributions of lasing thresholds for uniform pumping (dashed black lines) and partial pumping (solid red lines). Partial pumping increases lasing thresholds. The inset shows the *re-normalized* probability distribution (solid dark-red lines) for partial pumping. The rising slope of the first main peak is 4.5 times greater with uniform pumping than with partial pumping. (b) Probability distributions of thresholds normalized to the most probable threshold. Partial pumping redistributes lasing thresholds by destroying small-threshold modes and creating large-threshold modes. The number of large-threshold modes (found by the area under the curve for $n_i > 0.175$ or $n_i/n_m > 1.55$) is 25% of the total number of modes. The inset shows the shape of the main peak with partial pumping almost the same as that with uniform pumping but slightly narrower.

partial pumping, the slope is 4.5 times smaller than with uniform pumping (including the large-threshold tail for partial pumping gives a slope 6 times smaller). If the pumping rate is gradually increased from zero, the number of available lasing modes can be less with partial pumping. In Sec. 4 we discussed how the relative pump step $\delta P = \Delta P/P_i$ is smaller for larger P_i in experiments. The most probable threshold n_m gives a good representation of P_i by showing the increased lasing thresholds are a general occurrence and not limited to one random realization. The relative pump step $\delta n_i = dn_i/n_m$ may allow a finer tuning of the pumping rate, thereby making it easier to see modes begin lasing incrementally.

Although the absolute fluctuation of lasing thresholds does increase for partial pumping, the effect is different from the increased fluctuation shown for increased scattering strengths with uniform pumping [44]. Figure 5(b) plots the uniform and partial pumping distributions versus the thresholds normalized to their most probable value n_m . The inset of Fig. 5(b) reveals that the two distributions are nearly identical at smaller thresholds. Because there is no absorption, feedback from scattering in the unpumped region of the random structures still occurs. Thus, it is not surprising that the results are quite similar.

Even in this case without absorption in the unpumped region, the number of modes does change with partial pumping. For the 10000 realizations, a total of 81396 modes were found for uniform pumping and 67371 modes were found for partial pumping. The total number of modes with partial pumping is 17% less than with uniform pumping. If we assume only 96% of modes were successfully found with partial pumping (based on the test results), the total number of modes with partially pumping is 14% less. However, 25% of all modes with partial pumping are located in the large-threshold tail, as shown by the shaded area in Fig. 5(b). Thus, the number of *available* small-threshold lasing modes for partial pumping is roughly 35% less than for uniform pumping. With the number of available lasing modes reduced, the frequency spacing between them increases. The enlarged filled diamonds in Fig. 4(a) shows modes which

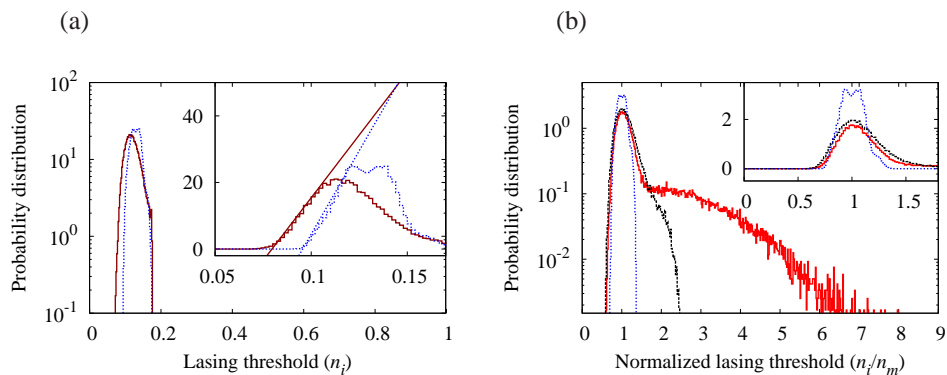


Fig. 6. (Color online) (a) Probability distributions of lasing thresholds for partial pumping without absorption (solid dark-red lines) and with absorption (dotted blue lines). The distribution without absorption excludes large-threshold modes and has been re-normalized. Absorption increases lasing thresholds. The inset shows the rising slope is roughly 1.3 times greater with absorption than without absorption. (b) Probability distributions of thresholds normalized to the most probable threshold for uniform pumping (dashed black lines), partial pumping (solid red lines), and partial pumping with absorption (dotted blue lines). The inset shows partial pumping with absorption narrows the main peak.

exist for uniform pumping but not partial pumping. These modes disappear, as described in [20], but the remaining modes still exist with relatively the same frequency k .

Figure 6(a) compares the threshold statistics for partial pumping ($\ell_G/L = 1/3$) with and without absorption in the unpumped region. The absorption length is $\ell_a = 170$ nm. The large-threshold modes have completely disappeared by adding absorption in Fig. 6(a). The large-threshold tail without absorption has been excluded in order to compare the distributions directly. We have found [46] that the large-threshold modes are spatially concentrated on one side of the pumping region (typically on the side with lower index contrast compared to the outside medium, i.e., the right side in this case). Thus, absorption added to this side of the structure effectively kills these modes.

With absorption in the unpumped region, lasing modes are confined to the pumped region. Thus, the number of modes is dictated by the effective system size $\ell_G + \ell_a$ which is roughly three times less than the uniform pumping case. We consider three times as many random structures when absorption is included to obtain comparable sampling. For the 30000 realizations, a total of 76673 modes were found for partial pumping with absorption (comparable to the 81396 modes found for uniform pumping with only 10000 realizations).

Figure 6(a) shows a noticeable bi-modal distribution for the case with absorption. This stems from the small number of modes within the wavelength range of interest ($500 \text{ nm} \leq \lambda \leq 750 \text{ nm}$) and the use of frequency-independent gain. The two peaks correspond to different mode numbers. The smaller-threshold peak is composed mostly of higher-frequency modes while the larger-threshold peak is composed of lower-frequency modes. There is not enough fluctuation in their thresholds to completely wash out the bi-modal distribution. Thus we take an average of the two most probable thresholds to find n_m . This results in $n_m = 0.129$ with absorption, which is nearly identical to the mean threshold $\langle n_i \rangle = 0.130$. n_m is 15% larger for partial pumping when absorption is included in the unpumped region. This increase of n_m shows the lasing threshold increase is a general occurrence and not limited to one random realization.

The standard deviation decreases from $\sigma = 0.023$ for partial pumping without absorption to

$\sigma = 0.015$ when absorption is included. This indicates the fluctuation of thresholds decreases when absorption is included. Furthermore, the inset of Fig. 6(a) shows the slope of the rising part of the re-normalized distribution for partial pumping. With absorption, the slope is 1.3 times greater (including the large-threshold tail without absorption means the slope with absorption is 1.8 times greater). Compared to the uniform pumping case where $\sigma = 0.012$, the absolute fluctuation of thresholds is still larger with partial pumping even when absorption is included. The rising slope of the distribution with absorption is roughly 3.4 times smaller than for uniform pumping.

Figure 6(b) compares the distributions normalized to n_m . In this case, when absorption is included, the distribution is narrower. Measuring the half-width σ_n for each case yields $\sigma_n = 0.232$ for uniform pumping, $\sigma_n = 0.200$ for partial pumping, and $\sigma_n = 0.145$ for partial pumping with absorption. Without absorption, the distribution narrows as well which may not be surprising if spatially inhomogeneous gain is considered to enhance scattering feedback from within the pumped region [19], thereby reducing the effective system size slightly.

6. Discussion and Conclusion

The spectral behavior with partial pumping was studied in weakly scattering random lasers. A FDTD-based method for solving the stochastic Maxwell-Bloch (SMB) equations was employed. Simulation results of a random system pumped uniformly and partially were compared. For partial pumping, the system was studied with and without absorption outside the pumped region. It was revealed that there are fewer lasing peaks with partial pumping and even fewer when absorption is added to the unpumped region. The resulting greater frequency separation between lasing modes makes them more distinguishable in the emission spectra compared to uniform pumping where modes often spectrally overlap.

The SMB simulations produce more accurate results than semiclassical laser theory because the spectral linewidth of lasing modes and emission fluctuations are included. Each peak in the emission spectra from the SMB simulations was found to correspond to a threshold lasing mode (TLM) calculated by the transfer matrix method with linear gain. Lasing threshold statistics were obtained for an ensemble of random structures for uniform pumping and partial pumping with and without absorption in the unpumped region. Gain saturation and noise were excluded so that the effects of partial pumping could be isolated. The statistical calculations simply specified a generic absorption length independent of any specific loss mechanism (such as reabsorption, scattering loss, etc.).

We identified two possible reasons why it is easier to see discrete lasing peaks with partial pumping: (I) a decrease in the density of possible lasing states (DLS) and (II) an increase in the fluctuation of lasing thresholds. With absorption in the unpumped region, the number of lasing modes is already known to scale with the size of the pumped region. Thus, the DLS can decrease drastically. Without absorption, it was found that the total DLS decreases only slightly (by roughly 14% compared to 67% with absorption). However, partial pumping results in the disappearance of some small-threshold modes and the creation of larger-threshold modes. With noise, it is usually seen that only the smaller-threshold modes appear in the emission spectrum. This redistribution of lasing thresholds results in a further decrease of the density of small-threshold lasing modes (35% compared to 14%). This decrease without absorption is not as great as that with absorption. However, the effect of absorption depends on the size of the pumped region ℓ_G . If the size of the unpumped region $L - \ell_G$ is less than the absorption length ℓ_a , the total number of modes with and without absorption may be similar.

The distribution of thresholds normalized to the most probable threshold narrowed with partial pumping. However, an increase in the fluctuation of absolute values of lasing thresholds for partial pumping occurred. The larger threshold separation also manifested itself in the smaller

rising slope of the threshold distribution. The number of modes within a given threshold range dn_i is thus smaller with partial pumping. The threshold fluctuations for partial pumping without absorption in the unpumped region were nearly twice as large as those for uniform pumping. With larger lasing thresholds, stronger pumping is required to reach lasing in partially pumped systems, making the amplified spontaneous emission (ASE) stronger. The SMB simulations show that noise tends to smear out the differences in thresholds as it constantly excites all modes within the gain spectrum. With partial pumping, all TLMs in the small-threshold regime resulted in well-defined peaks in the SMB emission spectra. This result, however, clearly depends on the absolute strength of the threshold fluctuations and the tunability of the pumping rate. Larger threshold fluctuations would make the selection of fewer small-threshold modes for lasing possible, even in the presence of noise. The tunability of the pumping rate, experimentally, depends on the lasing threshold P_t . Given a fixed pump step δP , the relative pump step $\delta P = \Delta P/P_t$ is smaller for larger P_t . The most probable threshold n_m gives a good representation of P_t . n_m was found to increase for partial pumping. Thus, a finer tuning of the pumping rate (smaller steps $\delta n_i = dn_i/n_m$) is possible. This facilitates the observation of an incremental increase of lasing modes with the pumping rate.

In conclusion, the density of possible lasing states (DLS) was found to decrease with a smaller spatial pump region. This, in combination with the larger threshold fluctuations, is likely to produce discrete lasing peaks in the emission spectrum. For partial pumping with absorption in the unpumped region, the DLS decreased according to the pump size directly. For partial pumping without absorption, the DLS decreased less dramatically but the threshold fluctuations increased more. Thus, threshold fluctuations play a larger role in partially pumped systems where no absorption exists in the unpumped region. Our findings provide qualitative explanation for the experimental observations of weakly scattering random lasers based on colloidal dye systems [10–12]. Our work may also be relevant for recently reported fibre random lasers [48,49] because they are extremely weak scattering one-dimensional random lasers with spatially inhomogeneous gain and loss. In those systems, the gain length is much larger than the scattering mean free path. Further study is needed to fully understand their lasing behavior. A quantitative verification of our findings in this paper requires systematic experimental studies, e.g., a systematic measurement of lasing threshold fluctuations with a varying pump area, mean free path, and absorption length outside the pump area.

Acknowledgments

We thank Prof. C. Vanneste for numerous discussions and pertinent suggestions concerning this manuscript. We also thank Prof. P. Sebbah and Dr. S. B. N. Bhaktha for stimulating discussions. This work is supported in part by the National Science Foundation under Grant DMR-0808937 and the Yale University Faculty of Arts and Sciences HPC Center.